The implementation of a computational fluid dynamics algorithm within the ESP-r system

J A Clarke, W M Dempster, C Negrão

ESRU, Energy Systems Division, Faculty of Engineering,
University of Strathclyde, Glasgow G1 1XJ.

email: esru@strath.ac.uk
phone: +44 141 552 4400 X3896
fax: +44 141 552 8513.

ESRU PhD student associated with Bolsista do CNPq - Brasília, Brasil

ABSTRACT

This paper describes the implementation of a computational fluid dynamic algorithm within the ESP-r building energy modelling system. While the implementation is specific to ESP-r the conflation approach is general and could be applied to other building performance appraisal programs. The paper also presents an example application to indicate the potential effects of the enhanced modelling resolution and some of the new issues to emerge.

INTRODUCTION

Building energy/environmental prediction based on computational modelling is receiving much attention at the present time: mathematical models, discretisation techniques and numerical methods are being refined, and application know-how is maturing. Building simulation (BSim), in which the building's distributed capacity and air volumes are discretised (the latter relatively crudely), and computational fluid dynamics (CFD), in which some fluid domain is finely discretised, are two significant development fields.

BSim conceives of a building's fabric, spaces, plant and systems as a network of time varying thermal/flow resistances linking different *finite volumes* each possessing thermal capacity. Mass and energy conservation equations are then established for each finite volume and solved simultaneously. In this way the conductive, convective, fluid flow, radiative and heat storage processes are explicitly modelled as the system responds to climate boundary conditions. Typically, the finite volumes are relatively large (e.g. 20 - 60 within a wall and 1 - 3 within a room) so that a medium sized office building might be represented by 2000 - 7000 conservation equations.

The CFD technique is essentially similar except that to the describing set of equations is added momentum conservation and a turbulence model so that the technique is applicable at the micro scale. Typically, the finite volumes are relatively small (e.g. 200 - 2000 within a single space) so that one room within the above office building might be represented by 600 - 6000 conservation equations.

Although the two techniques share a similar numerical basis, their focus is entirely different: BSim focusing on the constructions, engineering plant, inter-space air flow (including infiltration to external spaces) and the influence of users and control systems; CFD focusing on the mass, momentum and energy transport in a single fluid domain. In effect, the two systems are the mature

subjects of separate developments, each only emphasising one aspect of the problem while simplifying the other. As a result two principal limitations are evident in the context of building performance appraisal:

> BSim is deficient in its representation of local flow phenomena and room air to surface heat transfer. This may well lead to problems with the accurate estimation of surface temperature distribution, condensation risk and local thermal comfort.
>
> CFD is deficient in its representation of dynamic boundary phenomena, requiring surface temperature gradients and air handling plant momentum interactions as input. Paradoxically, this may well lead to a reduction in modelling realism despite the increase in modelling resolution.

By developing a system of combined functionality such problems can be overcome. From a mathematical viewpoint, the conflation of BSim and CFD represents a challenging problem, involving as it does a mix of partial differential equations typifying both the macro and micro scale conservation of mass, momentum, energy, turbulent quantities and, perhaps, species in a complex dynamic system. How best to achieve this conflation is the subject of this paper.

BSim and CFD COMPARED

Physically, the overlap between BSim and CFD occurs only in certain parts of the system being modelled. This translates to certain BSim-side fluid finite volumes, each of which can be considered as the computational domain for CFD. Hence the governing equations for BSim and CFD in the overlapping domain must be interpreted each against the other. For CFD the control equation is

$$\frac{\partial}{\partial t}(\rho\phi) = \frac{\partial}{\partial x_i}(J_\phi)_i + S_\phi \qquad (1)$$

where ϕ represents any transport variable (velocity components, temperature, etc.), $(J_\phi)_i$ is the convective and diffusive fluxes defined as

$$\Gamma_\phi \frac{\partial \phi}{\partial x_i} - \rho V_i \phi.$$

The transport variables, diffusion coefficient, Γ_ϕ, and the source term, S_ϕ, are given in Table 1 for each conservation equation. The integrated form of Equation (1) over a finite volume P assumes the following form

$$\frac{\partial}{\partial t}(\rho\phi V)_P = (J_\phi A)_{CS} + S_\phi V \qquad (2)$$

where V is volume, A is area, CS designates the control surface area and J_ϕ represents the convective and diffusive fluxes which are usually approximated as a function of the transport property differences evaluated at the center of P and its neighbours.

From the BSim viewpoint, the rate of storage of a transport property within a finite volume I is equal to the net flux exchange with surrounding volumes plus any generation of the property within the volume:

$$\frac{\partial}{\partial t}(\rho\phi V)_I = (J_\phi A)_{CS} + S'_\phi \qquad (3)$$

where ϕ is temperature, moisture content, etc. and S'_ϕ is a source of energy or mass generation. J_ϕ is the flux of the transport property at the surface, usually approximated as an interaction between I and other entities, say regions 1, 2, 3 and 4 representing conductive, convective and radiative flow-paths:

$$(J_\phi A)_{CS} = \sum_{j=1}^{N}(K_{j,I}(\phi_J - \phi_I)) \qquad (4)$$

where $K_{J,I}$ is a linearised flow conductance between volume j and volume I and t is time.

Equations (2) and (3) are the basis of the conservation equations for each finite volume comprising the system. They represent the mathematical consistency of BSim and CFD in a spatial overlap region. At the mathematical level, this overlap implies that combined functionality is possible, although several factors must also be taken into account when devising a conflationary mechanism. Firstly, the combined system matrix equation will be highly sparse and so any approach which requires explicit matrix formulation must be avoided. Secondly, each computational domain is already endowed with customised, and hence efficient, numerical processing schemes and, where possible, these should be retained. And thirdly, the software equivalent of these numerical schemes are tried and tested and should be built upon.

CONCEPTUAL BASIS OF THE CONFLATION APPROACH

Consider the overall matrix equation for some combined BSim/CFD system as built up from the repeated application of Equations (2) and (3) to the finite volumes of two overlapping regions in a system (e.g. a whole-building BSim model and a single room CFD model). The future time-moment coefficients matrix is then a large, sparse system as represented (say) by Figure 1. If established, this 'super-matrix' would require the square of the sum of the sub-system matrices for its storage - i.e. a system as represented by a combined BSim/CFD approach would require several times the matrix storage space when compared to the separate BSim and CFD cases. (Note however that within the present work this matrix equation is never established.)

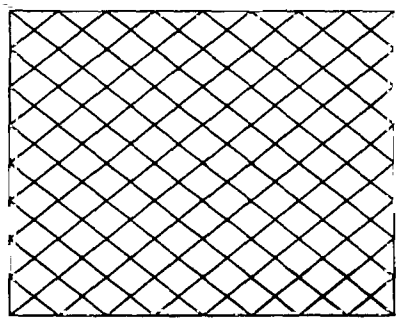

Figure 1: A BSim/CFD 'super-matrix'

The coupling coefficients of this overall matrix equation can be identified from the knowledge of the underlying theory. These coefficients, which are shown symbolically in Figure 2, link the different sub-system matrices - e.g. one for the overall BSim network flow balance and one for the CFD intra-space flows. Examples of these coupling coefficients include the momentum inputs corresponding to plant systems, infiltration and zone-coupled air flow, factors relating to the thermal boundary conditions and the surface convection coefficients.

Based on a previously elaborated technique (Clarke and Tang 1990), numerical techniques (Duff et al, 1986) can then be used to 'condense' these coupling parameters towards the matrix equation centre position as shown in Figure 3. Essentially this eliminates the sparsity by removing the null matrix elements.

Finally, as shown in Figure 4, modified BSim and CFD sub-system matrices are obtained

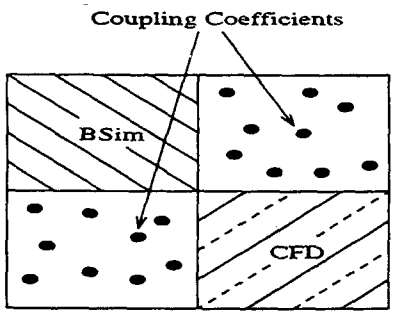

Figure 2: Coupling coefficients.

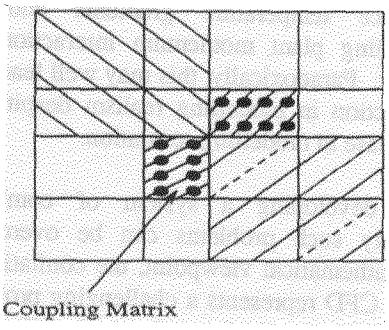

Figure 3: Condensing the super-matrix.

in a form which allows each sub-system to be solved independently, but in computational tandem, while ensuring that the results are identical to the simultaneous solution of the combined system.

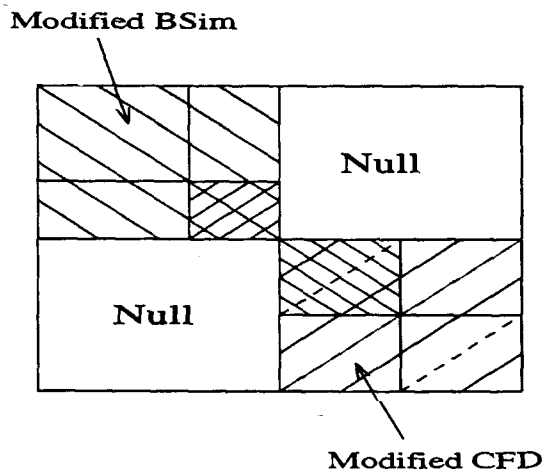

Figure 4: The modified BSim and CFD sub-system matrices.

The principal benefit of the approach is that existing BSim and CFD equation solvers can be retained and, by eliminating matrix equation sparsity, the computational burden can be

constrained to the pre-conflated level. The technique is applicable to problems of any size and is extensible to any domain involving large, sparse matrix equations.

ESP-r IMPLEMENTATION DETAILS

At the core of the approach is a method which allows ESP-r's existing network flow model to operate in tandem with a CFD algorithm[#1] which is fully integrated at the source code level.

Network Flow Approach

As shown in Figure 5, within ESP-r building and plant fluid flow is represented by a nodal network (Clarke and Hensen 1990) with the connecting branches representing physical components such as fans, ducts door-ways, cracks, etc. within which a pressure drop will occur. The representation is therefore constrained to the steady flow (possibly bi-directional) of an incompressible fluid along the connections which represent some leakage distribution when subjected to boundary conditions defining pressure and/or flow.

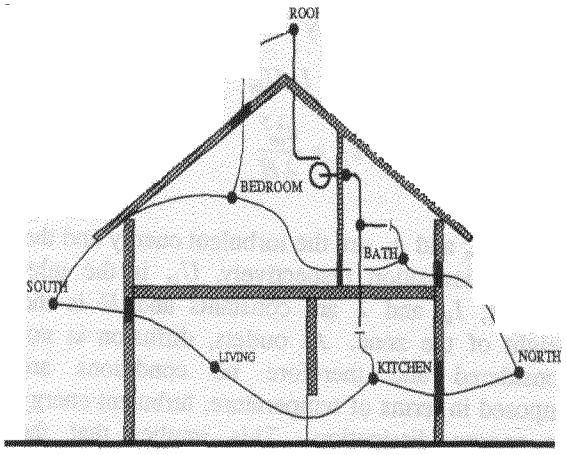

Figure 5: Example of an ESP-r fluid flow network.

An expression of the following type[#2] is used to represent the relationship between flow and pressure difference.

$$\dot{m}_{j,I} = f[(P_j - P_I)] \qquad (5)$$

where, $\dot{m}_{j,I}$ is mass flow rate through connection j, I and P is the pressure at nodes j and I (determined as the sum of static pressure, dynamic losses and stack effect).

Network solution proceeds as follows. Each fluid flow component, i, relates the mass flow rate, $\dot{m}_i$, through the component to the pressure drop, ΔP_i, across it. Conservation of mass at each internal node is achieved when the sum of the mass flows at the node is zero. Because these flows are non-linearly related to the connection pressure difference, solution requires the iterative processing of a set of simultaneous non-linear equations when subjected to a given set of boundary conditions. The technique used by ESP-r is to assign an arbitrary pressure to each internal node to enable the calculation of each connection flow from the appropriate connection equation. The internal node mass flow residuals are then computed from:

$$R_i = \sum_{k=1}^{K_{i,i}} \dot{m}_k \quad (kg/s) \qquad (6)$$

where R_i is the mass flow residual at node i for the current iteration, $\dot{m}_k$ is the mass flow rate along the kth connection to node i and $K_{i,i}$ is the total number of connections linked to node i.

The nodal pressures are then iteratively corrected and the mass balance at each internal node is re-evaluated until some convergence criterion is met. Within the technique a new estimate of the vector of all node pressures, $\mathbf{P}^*$, is computed from the current pressure field vector, $\mathbf{P}$, via

$$\mathbf{P}^* = \mathbf{P} - \mathbf{C} \qquad (7)$$

where the node pressure correction vector, $\mathbf{C}$, is determined on the basis of a simultaneous solution of a Jacobian matrix which represents the nodal pressure corrections in terms of all branch flow partial derivatives:

$$\mathbf{C} = \mathbf{R}\,\mathbf{J}^{-} \qquad (8)$$

#1 This algorithm is based on the 2D, steady state TEACH system (Gosman and Ideriah 1976), with extensions to enable 3D, transient operation. These extensions are reported elsewhere (Negrão 1994).

#2 ESP-r offers several expression types - such as power laws, quadratics and algorithmic. Such expressions are generally obtained empirically and are difficult to establish for intra-room flow. For this reason rooms are usually represented as one node (or two or three if buoyancy effects are to be modelling) implying the assumption of perfect air mixing.

where **R** is the vector of nodal mass flow residuals and $\mathbf{J}^{-1}$ is the inverse of the square Jacobian matrix whose diagonal elements are given by

$$J_{n,n} = \sum_{k=1}^{K_{n,n}} \left(\frac{\partial \dot{m}}{\partial \Delta P} \right)_k \quad (9)$$

and whose off-diagonal elements are given by

$$J_{n,m} = \sum_{k=1}^{K_{n,m}} -\left(\frac{\partial \dot{m}}{\partial \Delta P} \right)_k \quad (10)$$

where $K_{n,m}$ is the number of connections between node n and node m.

As noted by Walton (1988), there may be occasional instances of slow convergence, with oscillating pressure corrections on successive iterations. ESP-r employs the following technique to avoid this problem. By assuming a constant oscillation ratio, it is possible to extrapolate the corrections to an assumed solution:

$$P_i^* = P_i - C_i/(1-r) \quad (12)$$

where r is the ratio of C_i for the current iteration to its value in the previous iteration and $1/(1-r)$ is a relaxation factor. The extrapolated value of node pressure can be used in the next iteration. If it is, then r is not evaluated for that node in the following iteration but only in the one thereafter. In this way, r is only evaluated with unrelaxed pressure correction values. This process is similar to a Steffensen iteration (Conte and De Boor 1972) which is used with a fixed point iteration method for individual non-linear equations. The iterative correction method presented above gives a variable and node dependent relaxation factor. When the solution is close to convergence, Newton-Raphson iteration converges quadratically. By limiting the application of the relaxation factor to cases where r is less than some value, such as -0.5, it will not interfere with the rapid convergence.

CFD Approach

In this approach Equation (2) is discretised in time and space to give an algebraic conservation equation for each cell. The set of non-linear algebraic equations are then solved by the "Tri-Diagonal Matrix Algorithm" which sweeps the flow field line-by-line. The extensively used SIMPLE algorithm (Patankar 1980) solve the multi-dimensional mass and momentum transport equations. Stated briefly, this algorithm consists of an iterative procedure whereby an initial guesstimate of the pressures allows the momentum equations to be solved to give velocities. These velocities are then used to determine a pressure correction using a reformulated continuity equation. The pressure corrections are then used to establish new values of pressure and velocity and the process repeats until convergence is obtained. A staggered grid is employed by which the velocity components are placed at the boundary of the scalar variable (p, T, k and ε) cells. The grid, which can be uniform or non-uniform, is then arranged in such a way that the boundaries coincide with the finite volumes limits. This hybrid scheme is employed to approximate the convective and diffusive terms in Equation (2) and, along with linear under-relaxation factors, helps to eliminate numerical instabilities.

Close to a wall, laminar viscosity becomes more significant than eddy viscosity due to the damping effect of the wall. Because of this the turbulence model is not applicable and wall functions (Launder and Spalding 1974) are used to evaluate the velocity component parallel to the boundaries. At the inlets, a uniform distribution for the velocity components and the scalar variables is specified. Because turbulent energy and its dissipation are generally unknown at inlets, they are approximated by

$$k_{in} = I_{in} U_{in}^2 \quad (13)$$

$$\varepsilon_{in} = \frac{k_{in}^{1.5}}{\lambda H} \quad (14)$$

where, k_{in} and ε_{in} are the turbulent energy and the energy dissipation respectively, U_{in} is the inlet velocity, I_{in} and λ are constants and H is the height of the zone. At outlets, diffusion is not considered and therefore no conditions are imposed in terms of temperature, turbulent energy or energy dissipation. This implies that the internal flows are not influenced by the outlet conditions.

Convergence is achieved when the maximum relative residuals (among mass and momentum) are less than a given value. Relative residuals are computed as the sum of all individual cell residuals divided by the respective inlet source. In other words, the summation of mass residuals is divided by the inlet mass flow rate while the momentum residuals are divided by the inlet momentum.

Combined Network/CFD Approach

Within the combined approach as implemented within ESP-r, one or more network nodes are replaced by a gridded CFD domain, with the 'snipped' network reconnected to one or more of the CFD cells as illustrated in Figure 6.

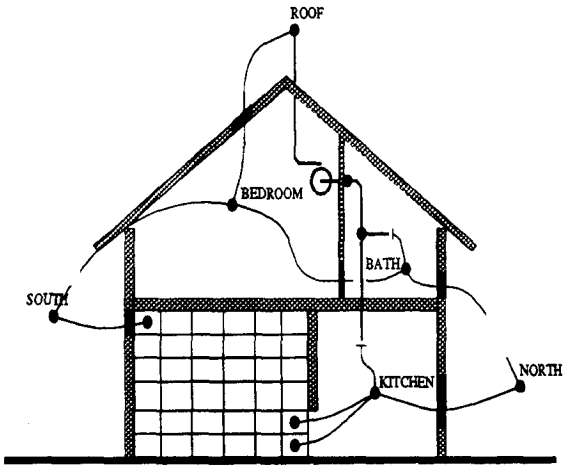

Figure 6: A connected flow network and CFD domain.

The actual coupling details are as illustrated in Figure 7a (located at the paper's end) which shows two possible scenarios: a one-to-one coupling to represent a window crack and a one-to-many coupling to represent a doorway.

The nodes L1, L2 and L3 represent the effect of the CFD domain on the network model. To allow each domain solution to be performed separately, the flow network must be decoupled from the CFD domain. Figure 7b shows how the domains are detached from each other. The sources or sink of mass ($\dot{s}_{L1}$, $\dot{s}_{L2}$ and $\dot{s}_{L3}$) on the decoupled network represent the air flow entering or leaving the finely discretised domain. If these sources or sinks of mass are considered known values, the flow network can then be solved. Pressures at the network nodes, including nodes L1, L2 and L3, and flow rates through the network, including the branches SOUTH-L1, L2-KITCHEN, L3-KITCHEN are then determined.

The $\dot{s}_{L1}$, $\dot{s}_{L2}$ and $\dot{s}_{L3}$ quantities, as evaluated by the CFD algorithm, are the product of the velocity components crossing the interface of the cell, densities and interface cell areas. The source/sink terms are thus computed by the following expression:

$$\dot{s}_k = \sum_j^m \sum_i^n (\rho V A)_{i,j,k}; \quad k = L1, L2, L3 \qquad (15)$$

where m is the number of cells which are connected to a mass flow network node, n is the number of interfaces of each cell (the interfaces at the opening boundary are not included), ρ is the air density, V is the velocity component at the cell interface and A is the interface area. If the flow is entering a cell it is considered positive while if it is exiting it is negative. a +ve $\dot{s}_k$ is therefore a source of mass and -ve a sink.

Operating separately, but in tandem, the solution of the CFD domain is carried out using the BSim-side generated boundary conditions. Within the implementation, two boundary conditions types are offered: imposed pressures at the coupling points (L1, L2 and L3) or imposed velocities (momentum) within the coupling branches (SOUTH-L1, L2-KITCHEN and L3-KITCHEN). The former type results in mass sources at inlets and mass sinks at outlets but with no momentum imposed at these points. While this is an inappropriate assumption in the case of large openings, it is appropriate when directional effects are small - such as with cracks where the dimension of the adjacent cell is significantly greater. The latter boundary type, imposed velocities at openings, is the most generic option but requires knowledge of flow direction in order to determine the correct coupling point. In this case the velocity is determined from the network-side flows (as computed for SOUTH-L1, L2-KITCHEN and L3-KITCHEN) divided by the product of sending node density and branch area.

Since the air flow between the coupling points is CFD-side dependent, while the pressures or momentum are network-side dependent, the two solvers much iterate until convergence is reached. Since the number of CFD-side equations for a single zone will usually be considerably greater than the number of equations for the building/plant flow network, the CFD-side controls the iteration - i.e. the network solution is initiated and completed for each CFD iteration.

AN EXAMPLE APPLICATION

The following example is intended to indicate the potential of the new method and demonstrate the expected magnitude of the differences in predictions between the combined approach and the network-only approach. The case studied is the house problem of Figure 6 with only relative simple models and coarse grids applied to allow investigation of the CFD network connection strategies. The two cells located at the openings are connected to two flow network

nodes, one external (south) and one located within the kitchen. Initially, buoyancy effects are not considered. The wind induced pressures at the external node are evaluated by means of pressure coefficients which differ with surface location. A non-linear relationship between mass flow rate and pressure difference is defined to represent the connection between flow network nodes and CFD cells:

$$\dot{m} = 0.65\, A \sqrt{2\,\Delta P}. \qquad (16)$$

Convergence of the CFD domain is only possible if the convergence criteria of the network domain is of the same order of magnitude. Low linear under-relaxation factors for the CFD momentum equations ($\alpha = 0.1$) were necessary to avoid boundary condition oscillations (when pressures and momentum as evaluated by the flow network). Approximately 600 iterations were necessary for a simulation which required approximately 200 iterations for a CFD only model.

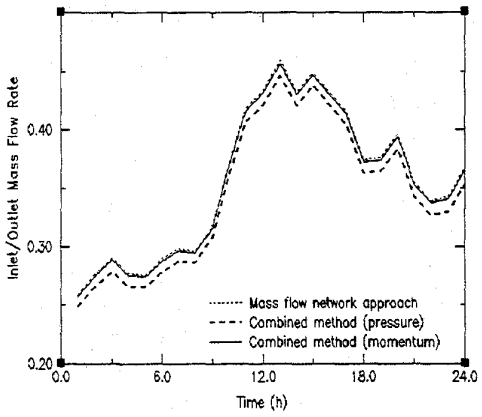

Figure 8: Mass flow rates - buoyancy not included.

A simulation was performed for a day in which the wind vector would induce a pressure at node SOUTH which was higher than that at node KITCHEN, giving a west to east air flow. Figure 8 shows a comparison between the inlet/outlet mass flow rates for the two possible boundary condition types - imposed momentum and imposed pressure. Note that due to incompressibilities the inlet and outlet mass flow rates are the same. For the case studied, the effect of the two boundary types was found to give results in the order of 3% different, which is insignificant.

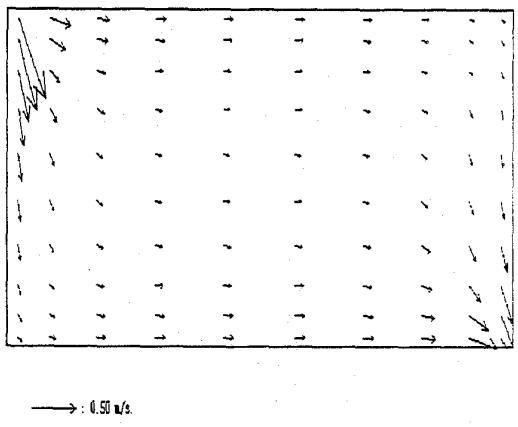

(a) imposed pressure, buoyancy excluded

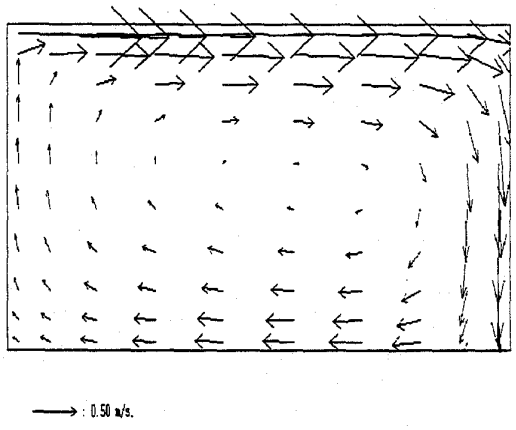

(b) imposed momentum, buoyancy excluded

Figure 9: Velocity fields for each boundary condition.

On the other hand, Figure 9 shows the velocity field at a given point in time, and for the two boundary condition types. As can be seen, the pattern of internal flow is different for each type. When momentum is imposed at the inlet, the flow presents a recirculation inside the room, which is not evident when the pressure is imposed.

In order to compare the combined model with the network flow approach, the flow network as shown in Figure 5 was simulated. The two boundary nodes (SOUTH AND KITCHEN) considered above are now connected to node LIVING by means of Equation (4). The LIVING node then represents the entire pressure field of the zone and no stack effect is considered. Figure 8 shows the differences between the air flows evaluated by the network method and by the

combined method. As can be seen the results are similar.

Buoyancy effects are now introduced in order to investigate the effect of natural convection on the flow. The difference in height between nodes SOUTH and KITCHEN induce stack pressures at nodes L1, L2 and L3. As expected, the flow is affected by natural convection. The inlet fresh air produces a recirculating flow inside the zone for either kind of boundary condition. This promotes a higher inlet air flow to the room as evident in a comparison of the flow rates of Figures 8 and 10: in the latter case the differences are more pronounced at the beginning and end of the day. At these times, the outside temperature is lower than the wall surface temperatures and natural convection is more significant. During other periods, the ambient temperature approximates to the wall surface temperatures and the buoyancy effect disappears.

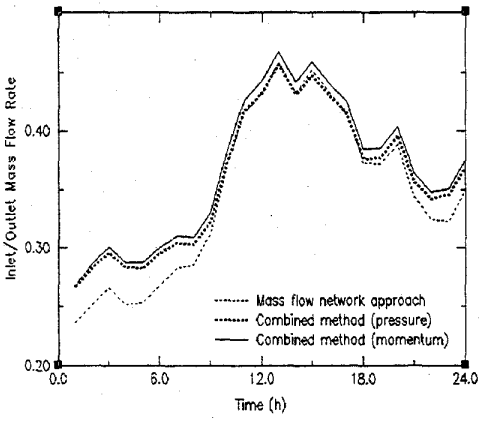

Figure 10: Mass flow rate - buoyancy included.

Figure 11 shows the new velocity field for each boundary condition type. For the case of imposed momentum at the inlet, the buoyancy-induced flow recirculation is not so evident, although the velocity is higher when buoyancy is taken into account. On the other hand, a recirculation flow in the upper part of the room is evident when pressure is imposed at the inlet. Although the two recirculating flows occur in opposite directions, both help to increase the inlet mass flow rate. For 3-D transient cases, convergence was not obtained for the fixed momentum case when buoyancy effects are included. The reason for this is the subject of further investigation.

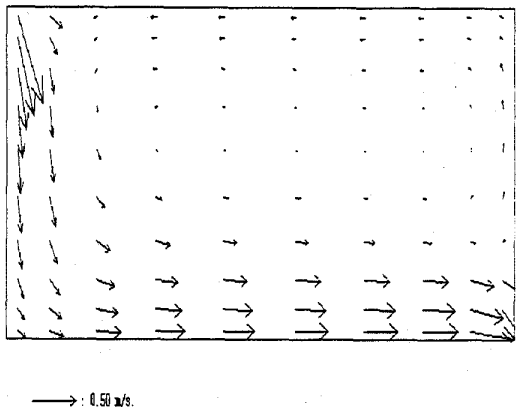

(a) imposed pressure, buoyancy included

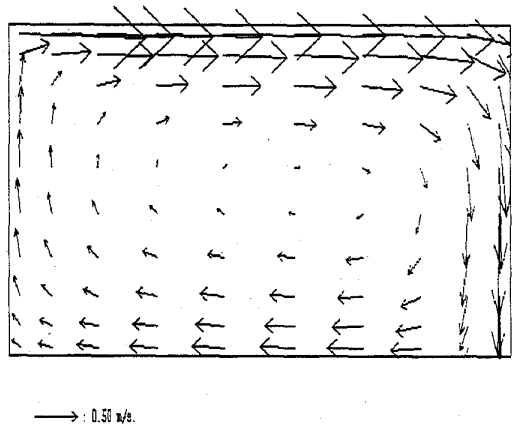

(b) imposed momentum, buoyancy included

Figure 11: Velocity fields for each boundary condition.

CONCLUSIONS

A method has been implemented within ESP-r by which BSim and CFD techniques are coupled. Preliminary studies indicate the advantages of this combined approach when compared with the network approach, even with relatively simple CFD models.

Investigations have indicated that the conflation of the two modelling approaches can be satisfactorily achieved by maintaining each method's separate solution algorithm. The connection between the two modelling approaches is then made within regions which each approach considers as its boundary condition. The overall system balance is then achieved through an iterative procedure. Careful consideration has to

be given to how the boundary conditions are implemented, especially for the CFD solution which is sensitive to the specifications of the inlet conditions.

Comparisons between simulations based on the combined method and a network only approach show that the latter is in reasonable agreement with the former when buoyancy is not consider. For the case studied, the inclusion of buoyancy reduced flow rates as predicted by the network-only approach but increased them in the combined approach.

Two boundary condition types - network-side, imposed pressure and momentum - for CFD momentum and continuity at the coupling points were analysed. It was found that the inside air flow is strongly dependent on the type selected. Momentum is the most appropriate for inlets if the incoming air flow is strong enough to disturb the flow inside the enclosure. Pressure is appropriate when the direction of the incoming air flow does not interfere with the internal flow.

REFERENCES

Clarke J A (1985) Energy Simulation in Building Design *Adam Hilger Ltd* Bristol and Boston.

Clarke J A and Tang D (1990) 'An Investigation of the Functional Conflation of Building Energy Simulation and Computational Fluid Dynamics', *Project Proposal to the UK SERC (now EPSRC)*, ESRU, University of Strathclyde.

Clarke J A and Hensen J L M (1990) 'An Approach to the Simulation of Coupled Heat and Mass Flow in Buildings', *Proc. 11th AIVC Conf.*, Belgirate, Italy.

Conte S D and Boor C de (1972) p*Elementary Numerical Analysis: an Algorithmic Approach* McGraw-Hill, New York.

Duff I S, Erisman A M and Reid J K (1986) 'Direct methods for sparse matrices' *Oxford Science Publication.*

Gosman A D and Ideriah F J K 1976 'TEACH-2E: A General Computer Program for Two-Dimensional, Turbulent, Recirculating Flows' *Imperial College.*

Launder B E and Spalding D B (1974) 'The Numerical Computation of Turbulent Flow' *Computer Methods in Applied Mechanics and Engineering* Vol 3 pp 269-289.

Negrão C O R (1994) 'Combining Mass Flow Network and CFD Approaches' PhD Progress Report, ESRU, *University of Strathclyde.*

Patankar S V (1980) 'Numerical Heat Transfer and Fluid Flow' McGraw-Hill, New York.

Walton G N (1988) 'Airflow Network Models for Element-Based Building Airflow Modeling' Technical Report, National Institute of Standards and Technology, Gaithersburg, USA.

Equation Type	ϕ	Γ_ϕ	S_ϕ
Continuity	1	-	-
Momentum	V_i	μ_{ef}	$-\frac{\partial p}{\partial x_i}+\frac{\partial}{\partial x_i}\left[\mu_{ef}\left(\frac{\partial V_j}{\partial x_i}\right)+\left(\frac{\partial V_i}{\partial x_j}\right)\right]-\rho g_i$
Energy	T	Γ_T	$\frac{q'''}{c_p}$
Species	C	Γ_C	$\dot{m}'''$
Turbulence Energy	k	$\frac{\mu_{ef}}{\sigma_k}$	$G-C_D\rho\varepsilon-G_b$
Energy dissipation	ε	$\frac{\mu_{ef}}{\sigma_\varepsilon}$	$C_1\frac{\varepsilon}{k}G-C_2\rho\frac{\varepsilon^2}{k}-C_3\frac{\varepsilon}{k}G_b$

$$\Gamma_T=\frac{\mu}{Pr}+\frac{\mu_t}{\sigma_T}\ ;\ \Gamma_C=\frac{\mu}{Sc}+\frac{\mu_t}{\sigma_C}\ ;\ \mu_{ef}=\mu_t+\mu\ ;\ \rho=\rho(T,C)$$

$$G_b=g\left(\beta_T\frac{\mu_t}{\sigma_T}\frac{\partial T}{\partial x_i}+\beta_C\frac{\mu_t}{\sigma_C}\frac{\partial C}{\partial x_i}\right)\ ;\ G=\mu_t\left(\frac{\partial V_i}{\partial x_j}+\frac{\partial V_j}{\partial x_i}\right)\frac{\partial V_i}{\partial x_j}$$

$$C_D=1.0\ ;\ C_1=1.44\ ;\ C_2=1.92\ ;\ \sigma_k=1.0\ ;\ \sigma_\varepsilon=1.3\ ;\ \sigma_T=0.9\ ;\ \sigma_C=0.9$$

Table 1: CFD transport variables, diffusion coefficients and source terms

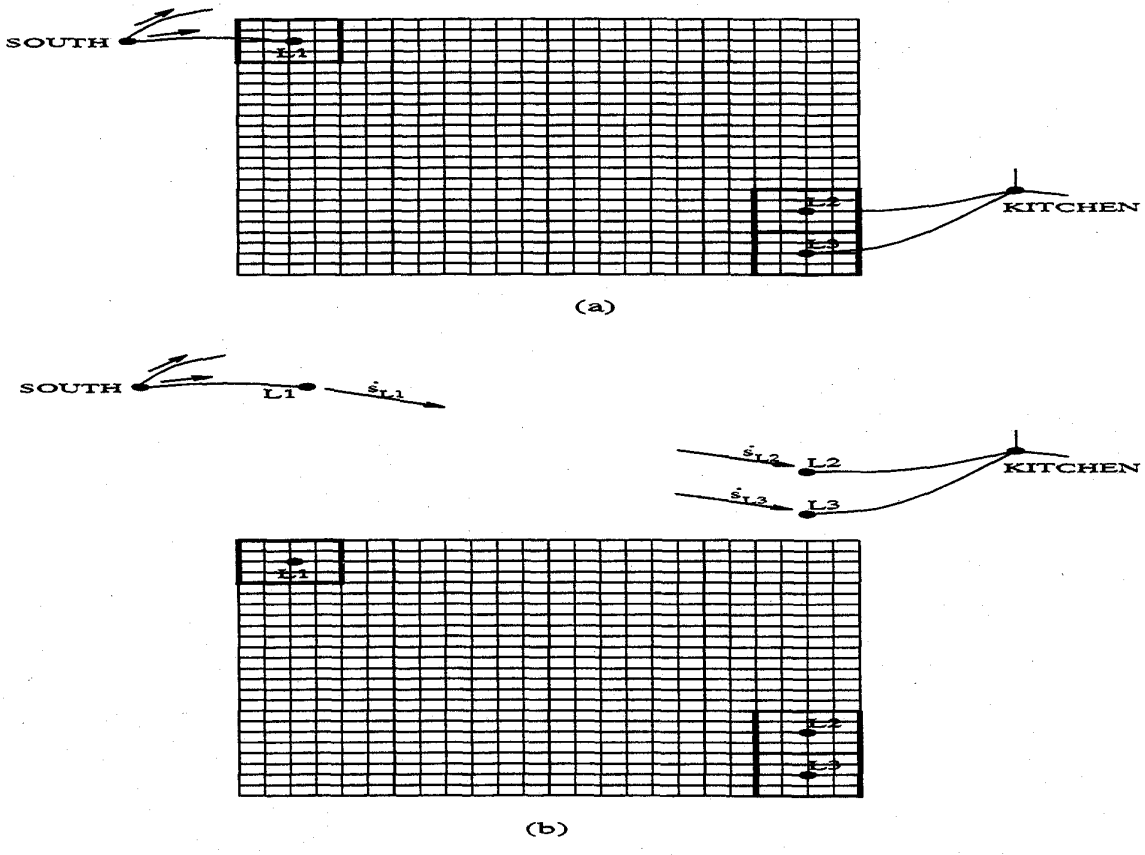

Figure 7: Node-to-grid cell coupling strategies.